

Impact of an Electric Locomotive on a Perfectly Smooth Railway Track in Terms of Rail Corrugation Formation

Jan Matej¹, Piotr Orliński^{1*}

¹ Institute of Vehicles and Construction Machinery Engineering, Faculty of Automotive and Construction Machinery Engineering, Warsaw University of Technology, ul. Narbutta 84, 02-524 Warsaw, Poland

* Corresponding authors' e-mail: piotr.orlinski@pw.edu.pl

ABSTRACT

Purpose of the article is to demonstrate that a high-speed electric locomotive, driven by asynchronous motors in a hollow shaft arrangement and swing-out couplings, can generate corrugation conditions on the surface of new and smooth rails on straight and curved track. Most studies carried out in this area is usually concerned with the response of the power train to kinematic excitation from a track where corrugations are already present. The novelty of the look presented in the article is to establish the influence of the vehicle's driveline and the parameters of a perfectly smooth formation track on the mechanism of corrugation. A four-axle EU11 electric locomotive, produced in Poland in the late 1990s, has been selected for analysis. A complete electro-mechanical model of the locomotive was built using the Vi-Rail software and prepared for simulation on straight and curved track. A non-linear model of wheel-rail contact was included and the contact forces were determined for the locomotive model in motion with the active power system. Unbalanced inertia forces generated by the scattering of stiffness characteristics of the coupling links, have been included to the propulsion system as an additional source of dynamic excitations. The complexity of the obtained results was influenced by the fact that simulation studies were carried out in both the time and frequency domains. The results obtained in the time domain were used to calculate the vertical and torsional vibration frequencies with respect to the driving wheelsets. One of the most important results of the simulation studies carried out is the determination of the effect of locomotive acceleration on the frequency of resonant torsional vibrations of the wheelsets in straight and curved track traffic.

Keywords: rail corrugations, electric locomotive, asynchronous motors, simulation studies, perfectly smooth railway track.

INTRODUCTION

Corrugations observed in real-life conditions are a kind of wavy wear on the upper surfaces of the rails, mainly on straight tracks or on gentle curves as shown in Figure 1(a). The rolling surface of the rail, formed in this way, becomes a source of additional high-frequency dynamic excitations transmitted from the track to the wheels of rail vehicles. In Poland, corrugations with wavelengths of 25 to 80 mm ('short' waves) and amplitudes of the order of hundredths of a millimetre are predominant [1]. It has been shown in the literature [2] that the occurrence of rail corrugation is closely related to the self-excited vibrations of

the wheel-rail system, and that the characteristic frequency of these vibrations is close to the characteristic frequency of the vibrations generated by the parameters of the already existing rail corrugation. In this literature the stochastic finite element method was used, investigating the sensitivity of parameters such as the elastic modulus and material density of the rail, the stiffness and damping of the track and the longitudinal creepage in the wheel-rail system as random parameters. According to [2] the following elements are necessary for the initiation and development of the corrugation process: the dynamic interaction between wheels and rails in the contact areas, the cyclicity of the vertical and longitudinal loads

exerted by the wheels on the rails, and the large longitudinal slips in the wheel-rail contact areas. Most of the available literature is concerned with studies of the mechanism of corrugation wavelength determination as a result of interaction between a wheel and a rail with a rough surface. In [3], data are presented showing that almost all inner rails of curved tracks with radii smaller than 350 m corrugate while corrugations rarely occur on outer rails. The author of [3] believes that rail corrugation is mainly caused by vibrations induced by the roughness present on the rails or by stick-slip vibrations of the wheelset. The test results presented in [4] were obtained for high-speed railways under the assumption that the rails are corrugated in the longitudinal direction. As the wheelset rolled over the corrugated area, the force responses of the wheel-rail system as well as the distribution of contact stresses on the rail surface were recorded in the time domain. Using the finite element method, the resonant vibration frequencies of the wheelset were determined here and the dependence of these frequencies on the acceleration acting on the selected axlebox was demonstrated. To investigate the growth mechanism of existing rail corrugations, the finite element method and a dynamic three-dimensional model of vehicle wheel-rail contact were used in [5]. Rail corrugations with different wavelengths and amplitudes were analysed. It was found that both longitudinal and vertical vibrations of the wheelset-track system have a dominant effect on the initiation and growth of corrugations. To investigate the non-linear dynamic responses of a heavy locomotive, a mathematical model of the vehicle was used in [6], taking into account the transfer of traction power from the electric motors to the axle of the wheelset via a gearbox with a large gear wheel rigidly mounted on the axle.

The model took into account the excitations from the corrugated rail, the non-linear wheel-rail contact and selected gearbox parameters. The vibration level of the vehicle and gearbox was found to increase with the amplitude of the rail corrugation.

In our article paper, an attempt was made to demonstrate that, in motion with an active drive system, a high-speed electric locomotive, driven by asynchronous motors in a hollow-shaft arrangement and swing-out couplings, can generate corrugation conditions on the surface of new and smooth rails on straight track and on a full curve of curved track. A four-axle electric locomotive EU11, designed to run trains at an operating speed of at least 200 km/h, was selected for the simulation studies – Figure 1b. This locomotive was manufactured in Poland in the late 1990s and has all the features of contemporary European designs, including propulsion provided by three-phase asynchronous motors with impulse starting.

MATERIALS AND METHODS

The elements of the real EU11 locomotive's primary and secondary suspensions were shown in Figure 2. Two steel coil springs 10 of the primary suspension and axle bearing housing guide 12 connect the wheelset 1 to the bogie frames 9. Between the bearing housing and the bogie frames, there are vertical hydraulic dampers 13. The locomotive's secondary suspension consists of Flexi-coil springs 11. Traction rod 18, connects the bogie frame to the locomotive car body. Between the frame of each bogie and the locomotive car body are located vertical hydraulic dampers 14 and longitudinal hunting dampers 15. The dampers 16 and 17 are used to suppress transverse vibrations of the bogie frame relative to the car body. The



Fig. 1. Simulation test objects. (a) example of corrugated wear on the rail surface [1]; (b) four-axle electric locomotive EU11 [7]

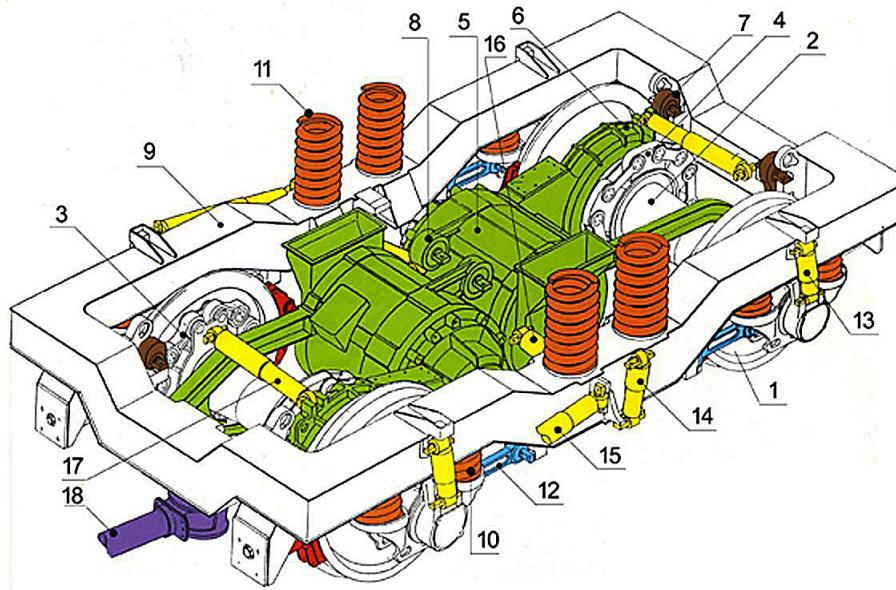


Fig. 2. Structural components of the EU11 locomotive [7]
 (a) sketch of the bogie structure; (b) primary suspension components

hollow shaft 2 is connected to the wheelset disc 1 by means of six-pinion clutch 3 and to the pinion gear drive wheel by means of clutch 4. The body of the traction motor, Joints 7 and 8 are used to rests the traction body motor 5 and the gearbox housing 6 on the front transverse beam and the centre cross member of the bogie. A sketch of the propulsion system was shown in Figure 3.

A mathematical model of the asynchronous motor was prepared in the form of a system of ordinary differential equations with constant

coefficients [8]. These equations described the relationships between armature and rotor magnetic fluxes, rotor speed and supply voltage. The stator and rotor windings and the winding flows along the air gap were assumed to be symmetrical, the winding resistances and reactances were assumed to be constant, the supply voltage waveform was assumed to be sinusoidal and the operating point of the magnetic circuit was assumed to be in the linear part of the magnetisation characteristic. However, the effects of hysteresis, saturation,

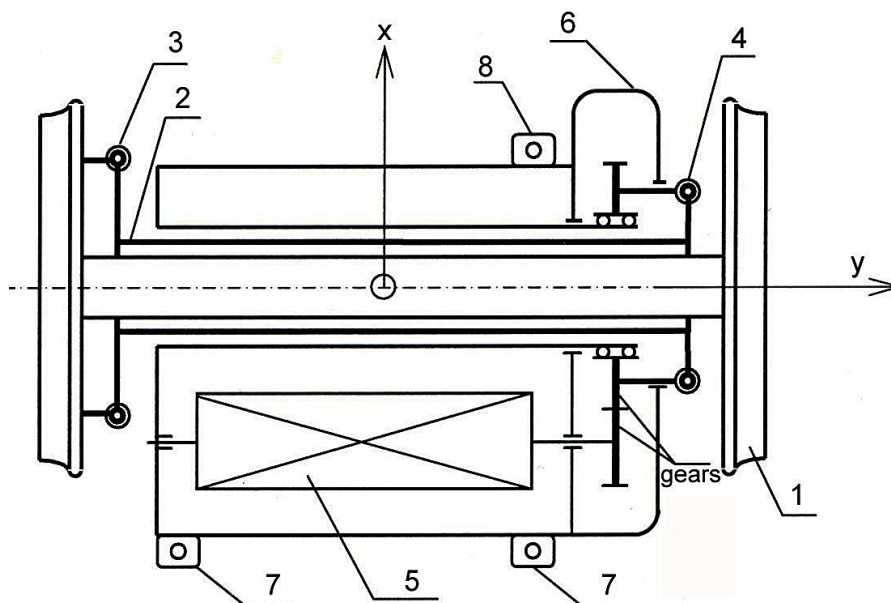


Fig. 3. Sketch of the propulsion system

anisotropy and losses on the eddy currents of the magnetic circuit were neglected. The final result was an equation relating the electromagnetic torque developed by the asynchronous motor:

$$M_e = \frac{3pL_m}{2(L_s L_r - L_m^2)} [\psi_{s\beta}^{(k)} \psi_{ra}^{(k)} - \psi_{sa}^{(k)} \psi_{r\beta}^{(k)}] \quad (1)$$

and the equation of rotation of the motor rotor:

$$J_e \frac{d\omega_m}{dt} = M_e(t) - M_m(t) \quad (2)$$

The following designations are introduced in equations 1 and 2: p - number of pole pairs of the asynchronous motor; J_e - reduced to the motor shaft moment of inertia of the system and rotor of the asynchronous motor; M_e - electromagnetic torque of the motor; M_m - mechanical torque reduced to the motor shaft; L_s - inductance of the stator windings; L_r - rotor winding inductance; L_m - magnetising inductance; $\psi_{sa}^{(k)}$ - magnetic flux associated with the successive phase of the stator; $\psi_{ra}^{(k)}$ - magnetic flux associated with the successive phase of the rotor; r_s - stator winding resistance; r_r - rotor winding resistance. The electrical part of the propulsion system of the locomotive under test consisted of four asynchronous motors and DC converters with a voltage of 3000 V. The DC current, taken from the catenary, was converted into three-phase AC current of adjustable voltage and frequency by means of an inverter. A PWM method was used to control the operation of the asynchronous motors by adjusting the frequency f and the voltage U supplying the asynchronous motor stator. With such control, with increasing motor speed, initially the torque has a constant magnitude and the power increases linearly. Thereafter, the motor power is constant and the torque decreases hyperbolically. The condition was imposed, ensuring

a constant value of drive torque, and P , allowing a constant value of power. A simulation, electro-mechanical model of the locomotive was built in the Vi-Rail software - [9]. All mechanical members of the simulation model, having geometry and mass, were treated as perfectly rigid bodies, connected to each other by kinematic pairs. The position of each member was described by 3 Cartesian coordinates and 3 Euler angles relative to a global, stationary reference system associated with the earth. This resulted in a simulation model of a locomotive with 152 degrees of freedom. The synchronous frequency was assumed to be 50 Hz and the DC catenary voltage was assumed to be 3000 V. The control of the asynchronous motors in the simulation model consisted of determining the control frequency f , the rise time of the control frequency and the rise time of the control voltage U . The structure of the locomotive model including the car body, bogie frames, wheelsets, traction motors, drive systems, suspension components and traction rods transmitting tractive forces from the bogies to the car body, is shown in Figure. 4. The index specifies the wheelset number.

A phenomenological model of the locomotive, taking into account the stiffnesses of the primary and secondary suspension springs and traction rods in the horizontal plane, is shown in Figure 5. The longitudinal and transverse axle-guiding stiffnesses of the wheelsets within the bogies are denoted by the symbols k_{ax} , while the longitudinal stiffnesses of the traction rods are denoted by the symbols k_{tr} and k_{trr} for the front and rear bogies respectively. The stiffnesses of the secondary suspension are described in the same way, using the capital letters K . Figure 6 shows a sketch of

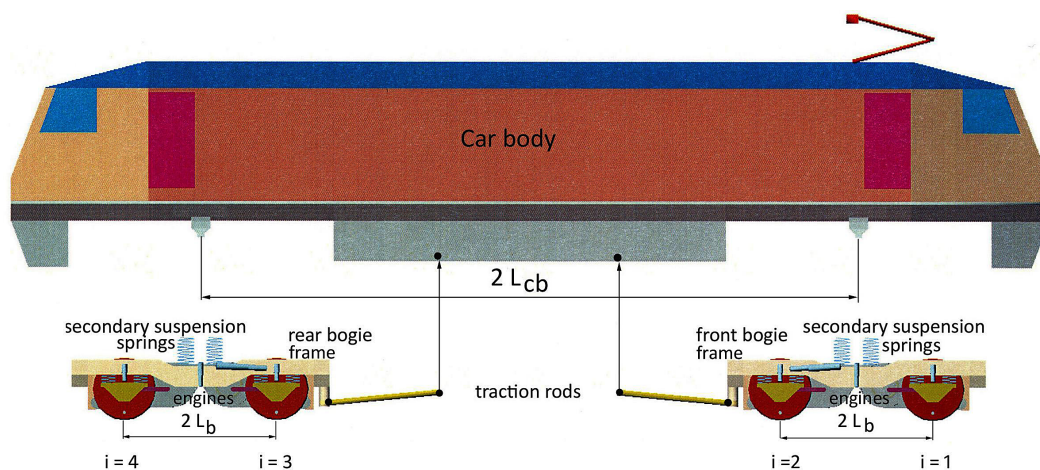


Fig. 4. Structure of the simulation model of a locomotive [9]

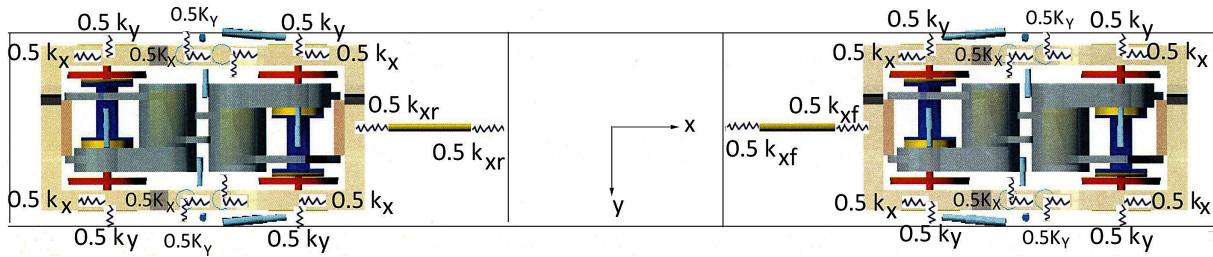


Fig. 5. Phenomenological model of the locomotive, including the stiffness of the primary and secondary suspension springs and traction rods in the horizontal plane [9]

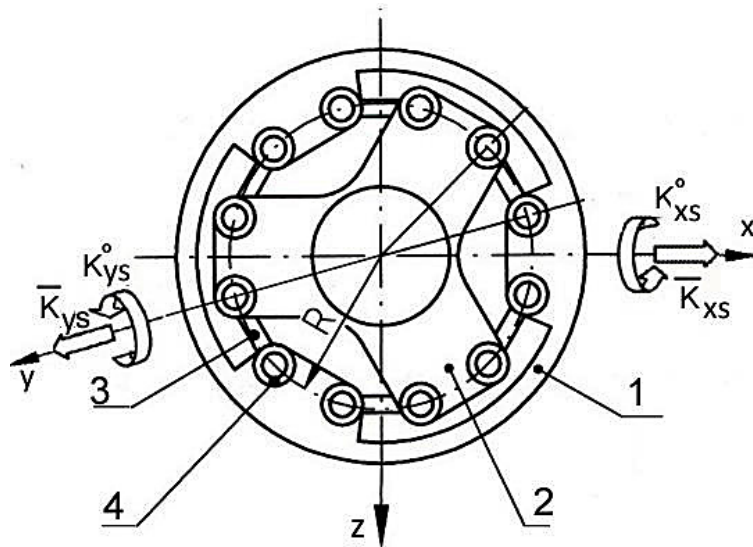


Fig. 6. Six-legged swing-out coupling of a locomotive [10]

six-legged swing-out coupling being a mechanical part of a locomotive drive system [10]. The structure of the coupling consists of passive component 1, active component 2, six links 3 set on the radius R and twelve metal rubber bushings 4.

For curved track, three sections were considered: a 200 m long straight track section, a 100 m long transition curve and a 200 m long full curve section with a cant of 150 mm and a radius of 300 m. The non-linear S1002 profiles of the wheels and 60E1 rails with a gradient of 0.025 rad were taken into account [9]. Knowing the coordinates of the centres of gravity of the individual model members, their masses and mass moments of inertia, the Vi-Rail software created and solved a system of differential-algebraic equations in each calculation cycle. The calculation of the non-elliptical shapes of the contact areas between the wheels with the rails was carried out by the WRGEN procedure based on Kalker's non-linear rolling contact theory [9]. Displacements, velocities, accelerations, forces acting on individual

components of the locomotive model as well as the vertical and tangential forces in the wheel-rail contact areas were determined. Interpretation of positive feedbacks of tangential forces in wheel-rail contact areas is presented in Fig. 7. In the remainder of this article, the terms outer rail/inner rail refer to curved track and are used interchangeably with the terms high rail/low rail.

During the movement of a locomotive model with an operating drive system in which there is a scatter in the stiffness characteristics of the coupling links, pulsations of unbalanced F_R inertia forces in the vertical, longitudinal plane of the clutch are generated. According to [10], it was assumed that the forces would not exceed 0.5% of the static vertical pressure of the locomotive wheel on the rail:

$$|F_R| \leq 0.005 \cdot Q_s \quad (3)$$

The numerical values of geometric dimensions, stiffness, damping, masses and mass moments of inertia of all components of the locomotive model

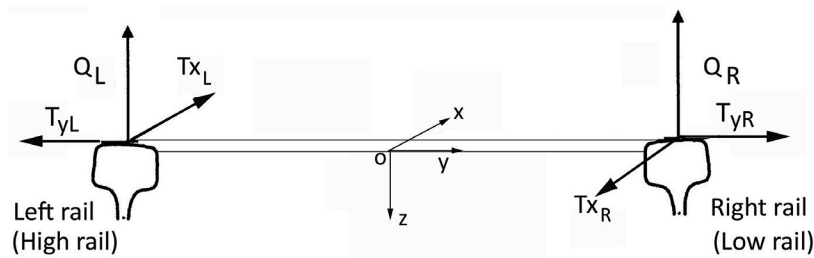


Fig. 7. Interpretation of positive feedbacks of tangential forces in wheel-rail contact areas

are given in Table 1. Data for the asynchronous electric motors are collected in Table 2. Table 3 contains the railway track parameters.

The simulation studies took into account also the locomotive’s fundamental resistance to movement. Formulas developed by COBiRTK (Central Railway Research and Technology Development Centre) were used for this purpose [10].

RESULTS

Increasing the speed of the locomotive model on straight and curved track was done with accelerations belonging to the value range

of 0.5 to 1.2. This required the adoption of a specific set of parameters controlling the operation of the electric motors. The numerical values of parameters, necessary to achieve the target speed of 63 on straight track and a speed of 19 on a full curve with a radius of 300 m with an acceleration of 0.6, are given in Table 4.

The simulation model of the locomotive was used to collect numerical values for the vertical and tangential forces in the wheel-rail contact areas. In the movement of the locomotive model with an acceleration of 0.6 each traction motor produced a driving torque of 2150 Nm on the straight track and of 2890 Nm over a full curve. In the remainder of this article, the indices *i* and

Table 1. Main numerical parameters of the reference locomotive model [7]

Designations	Parameter	Value/unit
$2L_{cb}$	Locomotive base	12.6 m
$2L_b$	Bogie base	2.65 m
M	Total locomotive mass	82000 kg
M_{cb}	Car body mass	50580 kg
M_{wst}	Wheelset mass	1950 kg
M_b	Bogie frame mass	2120 kg
r	Nominal wheel radius	0.55 m
i	Gear ratio	1:3.65
M_{du}	Integrated drive unit mass	3394 kg
M_{Hs}	Hollow shaft mass	450 kg
k_z	Vertical stiffness of primary suspension	1.88 MN/m
K_z	Vertical stiffness of secondary suspension	0.690 MN/m
k_x, k_y	Longitudinal/transverse primary suspension stiffness	1.034/2.083 MN/m
K_x, K_y	Longitudinal/transverse secondary suspension stiffness	0.413/0.137 MN/m
k_{xp}, k_{xr}	Longitudinal stiffness of the traction rod	10 MN/m
c_{xp}, c_{xr}	Longitudinal damping of the traction rod	25 kNs/m
c_x, c_y, c_z	Primary suspension damping coefficients in the directions X, Y, Z	30 kNs/m
C_x, C_y, C_z	Secondary suspension damping coefficients in the directions X, Y, Z	30 kNs/m
C_{HX}	Hunting damping coefficient	160 kNs/m
C_{1bY}	Lateral damping coefficient of primary suspension	80 kNs/m
C_{2BX}	Lateral damping coefficient of secondary suspension	30 kNs/m

Table 2. Numerical parameters of asynchronous electric motors [8]

Designations	Parameter	Value/unit
p	Number of motor pole pairs	3
J_e	Reduced moment of inertia of the drive system and motor rotor on the motor shaft	1000 kg*m ²
L_s	Stator winding inductance	0.00471605 H
L_r	Inductance of the rotor windings	0.00479105 H
L_m	Magnetising inductance	0.0031007 H
R_s	Stator winding resistance	0.03876 Ω
R_r	Rotor winding resistance	0.02133 Ω
R	Seating radius of coupling links	0.345 m
\bar{K}_{yS}	Clutch stiffness in axial direction	987 kN/m
\bar{K}_{xS}	Clutch stiffness in radial direction	135500 kN/m
K_{yS}°	Angular stiffness of the clutch in the axial direction	28932 kNm/rad
K_{xS}°	Angular stiffness of the clutch in the radial direction	71 kN/rad

Table 3. Railway track parameters [9]

Designations	Parameter	Value/unit
m_t	Unit rail mass	60 kg/m
m_s	Mass of railway sleeper	500 kg
$L_{sd}+L_{gt}$	Spacing of sleepers/rail gauge	0.60 m / 1.435 m
E	Young's module	2.1 E 11 Ns/m ²
ν	Poisson's ratio	0.27
μ	Coefficient of friction between wheel and rail	0.36
\bar{k}_{zL}	Vertical stiffness of the rail in the vertical direction	5.0 E7 N/m
\bar{k}_{yL}	Vertical stiffness of the rail in the transverse direction	4.3 E7 N/m
\bar{c}_z	Damping factor of the rail in the vertical direction	0.2 E6 Ns/m
\bar{c}_{yL}	Damping factor of the rail in the transverse direction	0.24 E6 Ns/m
k_H	Hertz contact stiffness coefficient	1.0 E9 N/m
c_H	Hertz contact damping coefficient	1.0 E4 Ns/m

Table 4. Numerical values of control parameters for asynchronous motors in motion on straight and curved track [9]

Straight track				Curved track with radius of 300 m			
$v_{max} = 63 \text{ m/s}$				$v_{max} = 19 \text{ m/s}$			
$f(\text{Hz})$	$U(\text{V})$	$t'_i(\text{s})$	$t'_j(\text{s})$	$f(\text{Hz})$	$U(\text{V})$	$t'_i(\text{s})$	$t'_j(\text{s})$
200	3000	100	25	60	3000	30	25

j are used to identify the individual wheels of the locomotive model and the associated vertical and tangential forces. Index i indicates the axle number of the wheelset, while index j identifies the wheel in a given wheelset. The vertical pressures on the selected rail locations were exerted first by the wheels of the first axle and then by the wheels of the three subsequent axles. Figure 8 shows the numerical values of the vertical pressures of the

wheels on the rails of the model moving at 63 on straight track in the situation of an active drive system. The black colour indicates the vertical pressures in the absence of scatter in the stiffness characteristics of the coupling links, while the red indicates the increments of normal pressures caused by the unbalanced inertia forces F_R coming from the clutch. The numerical values of the longitudinal tangential forces and their increments

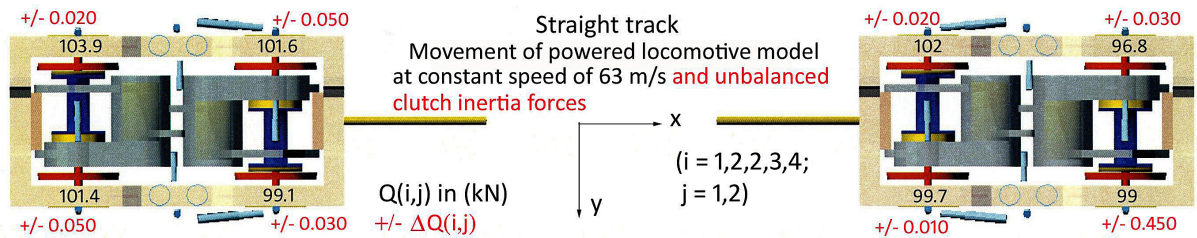


Fig. 8. Numerical values of the vertical pressures) exerted on the rails of the straight track by the wheels of the locomotive model with active propulsion system and their increments caused by the unbalanced inertia forces generated by the clutch

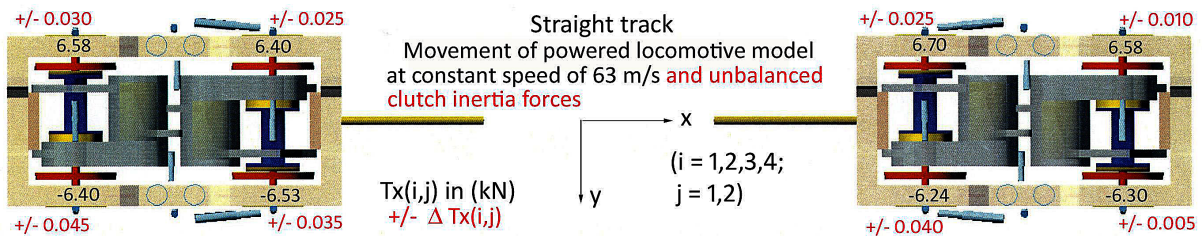


Fig. 9. Numerical values of the longitudinal tangential forces arising in the wheel-rail contact areas on straight track for the case of an active drive system and their increments caused by unbalanced inertia forces

induced by the unbalanced inertia forces are shown in Figure 9. The longitudinal tangential forces generate a couple of torsion moments M_T for the axle of the wheelset. Values of the vertical pressures of the wheels on the perfectly smooth rails of a full curve track with a radius of 300 m and the longitudinal tangential forces are shown in Figure 10 and Figure 11. Again the red colour indicates the increments of these forces caused by the unbalanced inertia forces F_R .

The non-linearity of the wheel-rail contact is evidenced by the shapes of the contact areas. They are presented graphically in Figure 12 and Figure 13, supplemented by numerical values of the contact areas created when the locomotive model moves along the straight or curved track with a full curve of 300 m radius. Values of the electromagnetic moments M_e and tangential forces were the input data for the calculation of the

vertical and torsional vibrations frequency of the wheelsets in motion with a given acceleration. The calculations in the frequency domain were reduced to the determination of the eigenvalues of the track-wheelset system. The results for the straight track and full curve with the radius of 300 m are shown in Figure 14 and Figure 15.

DISCUSSION

It was shown that during the transmission of driving moments to the wheelsets of the electric locomotive model, vertical loads and tangential forces are cyclically transferred to the rails at time intervals dependent on the speed of the model. On the straight track, all wheelsets aligned close to the track centre line. As a result, all wheel-rail contact areas are located in

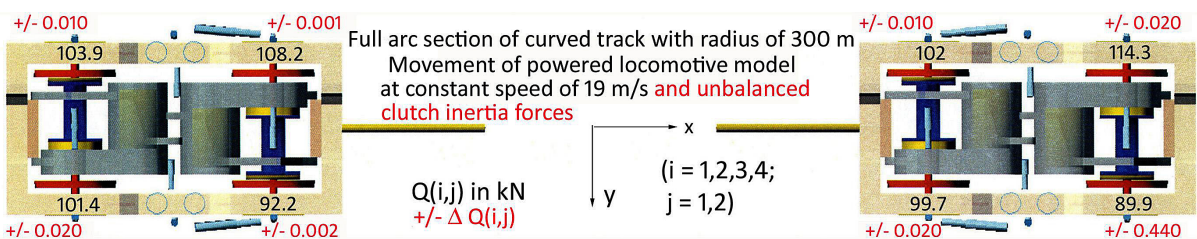


Fig. 10. Numerical values of vertical wheel pressures on the rails on a full curve of curved track with a radius of 300 m for an active drive system

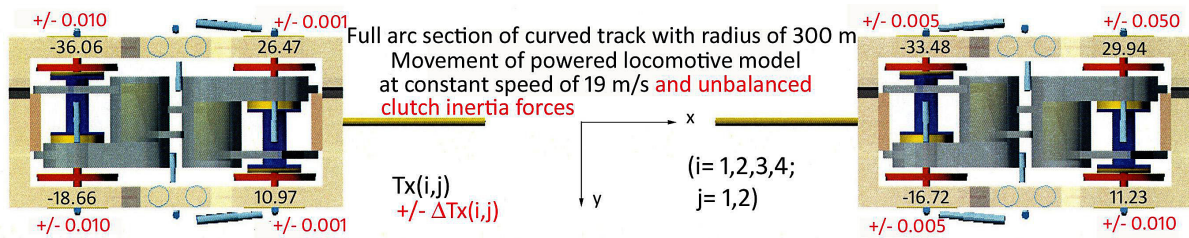


Fig. 11. Numerical values of the longitudinal tangential forces arising in the wheel-rail contact areas in the case of an active power train and their increments caused by unbalanced inertia forces on a full curve of curved track with a radius of 300 m

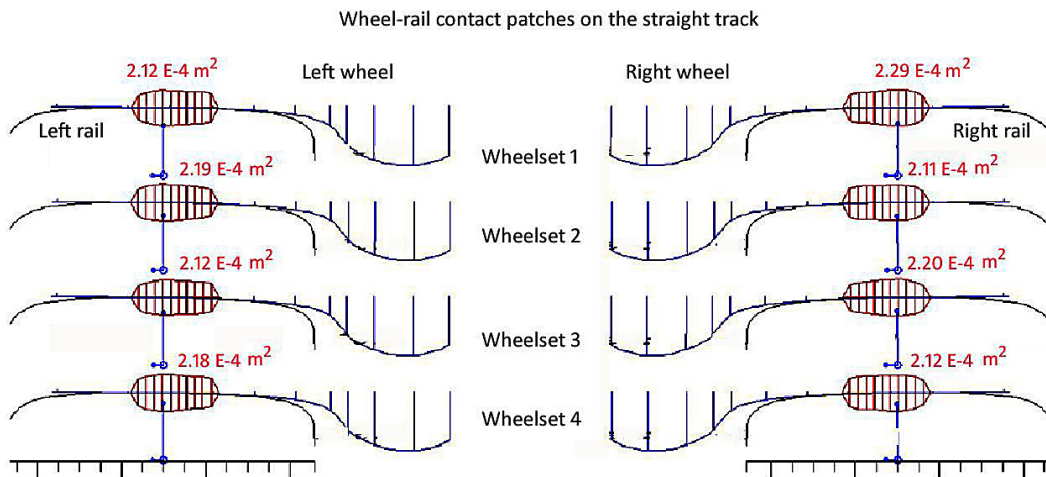


Fig. 12. Shapes, surface areas and positions of the wheel-rail contact patches of the locomotive model in straight track movement

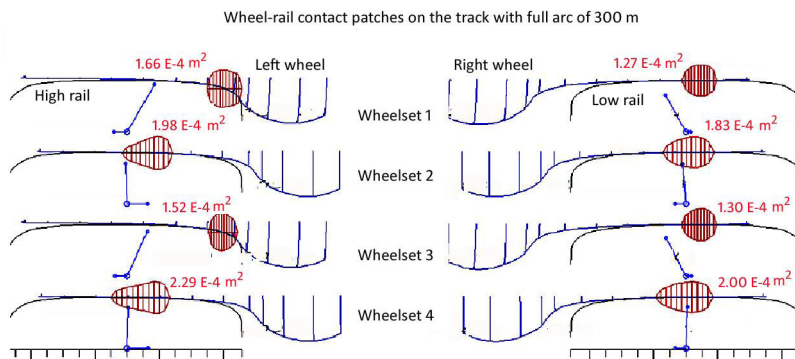


Fig. 13. Shapes, areas and positions of wheel-rail contact patches of a locomotive model on a full curved track curve with a radius of 300 m

the middle of the upper rail surface (Figure 10). A single load cycle of a given area of the straight rail consisted of four values of vertical forces exerted by successive wheels (Figure 12). At 63 , the rail on the left side of the straight track was loaded by successive wheels of the locomotive in a cycle of forces 96.8 kN, 102 kN, 101.6 kN, 103.9 kN, while the rail on the right side of

the track was loaded in a cycle of the following forces 195.8 kN, 201.7 kN, 200.7 kN, 205.3 kN. On a curved track with a radius of 300 m, the vertical pressures exerted on the outer rail by the wheels of wheelsets numbered 1 and 3 significantly exceed the loads on the inner rail (Figure 16). These wheelsets move outwards as much as possible relative to the centre line of the track,

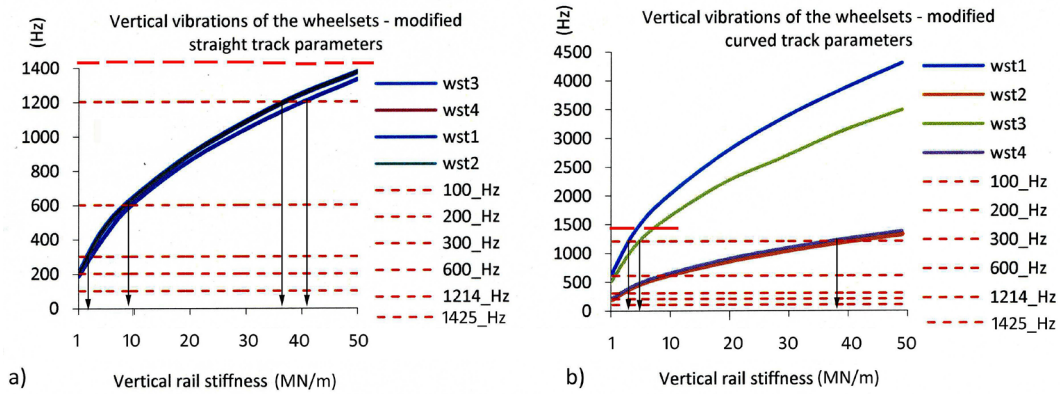


Fig. 14. Vertical natural frequencies for successive wheelsets of the locomotive model calculated as a function of rail vertical rail stiffness in the longitudinal vertical plane: (a) straight track; (b) complete curved track curve with a radius of 300 m

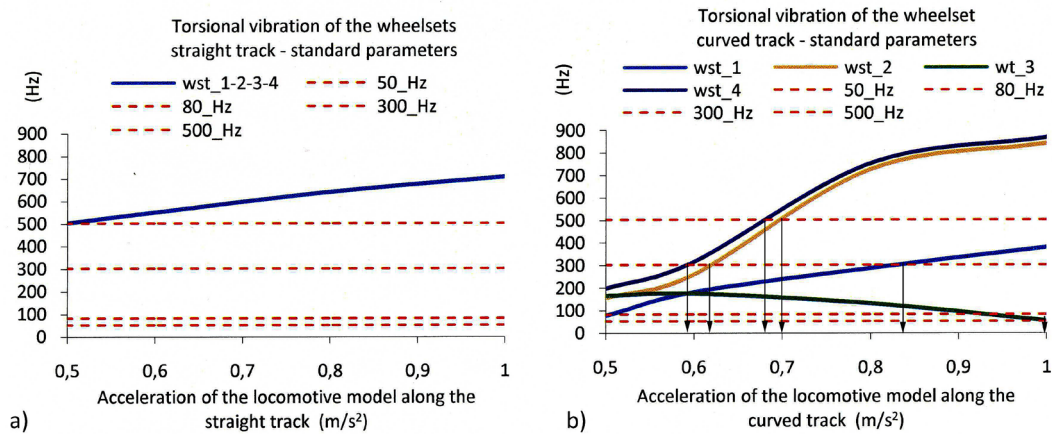


Fig. 15. Torsional frequencies of the wheelsets of the locomotive model in a function of the acceleration of the locomotive model: (a) straight track; (b) complete curved track curve with a radius of 300 m

resulting in large contact angles and large wheel angles of attack on the outer rail. The other two wheelsets position locates close to the track centre line and the contact angles of their wheels to the high rail are small (Figure 11). Such a configuration of the locomotive wheelsets means that on curved track, the top surface of the high rail is loaded only by the wheels of wheelsets 2 and 4, while the top surface of the low rail is loaded by wheels of all four wheelsets. This is one of the reasons explaining the fact that corrugation occurs mainly on the inner rail in the case of curved track.

It has been shown that the scatter of clutch stiffness does not significantly affect the dynamic action of the locomotive wheels on the rails if it is within acceptable limits. It was found that the pulsations of unbalanced inertia forces generated by the clutch in the vertical longitudinal

plane, increased the vertical wheel pressures on the rails by a maximum of about 0.5%. Knowing the values of the vertical wheel pressures on the rails and the areas of contact, the normal stresses were determined according to Hertz's linear contact theory. In each of the considered cases, the normal stresses significantly exceeded the maximum permissible value of 300. The peak values of these stresses on the straight track were of the order of 700. Similar normal stress values also occurred on the full curve of the track, but only for the second and fourth wheelsets. The wheels of the first and third axles exerted pressures on the rails generating rail normal stress values of up to 1000. These results coincide with those of the study presented in [4]. A similar agreement with [4] was also obtained for resonant frequencies.

Vibrations with resonant frequencies were recorded for the rail vertical stiffnesses in the

range from 1E6 N/m to 50E6 N/m. For standard value equal to 50E6 N/m, the natural frequencies of the wheelset vibrations in the vertical plane were outside the range of resonant frequencies for both the straight track and the full curve with a radius of 300 m (Figure 14). The resonant vertical vibration frequencies of the wheelsets only appeared when the vertical stiffness of a single rail in the longitudinal vertical plane is less than 5E7 N/m. For both straight and curved track, the most unfavourable situation occurs when the value of the aforementioned track stiffness is close to 1E6 N/m. The results of the calculations, concerning the numerical values of the natural frequencies of the wheelset – track system, are in accordance with those presented in [2] or [5] and confirm the direct influence on the possibility of corrugation formation. However, it should be noted that, contrary to the assumptions of the article presented here, the test scenarios described in [2], [5] and [6] were based on the assumption that the rails are undulating and that existing corrugations are the source of kinematic forcing from the track. While appreciating that a mathematical model of the vehicle incorporating the transfer of traction power from the electric motors to the axle of the wheelset via a gearbox was used in [6] to investigate the non-linear dynamic responses of the heavy locomotive, we note that the type of system considered is not typical of high-speed vehicles. In the simulation study scenario presented by us, an electro-mechanical drive system suitable for high-speed locomotives is included.

On analysed curved track the leading wheelsets, i.e. the first and third wheelsets in the direction of movement of the model locomotive, moved to the outside of the track centre line up to the contact between the wheel flanges and the high rail. This resulted in a multiplication of the vertical natural frequencies of these wheelsets (Figure 14b). It was also shown, that values of vertical and torsional vibrations frequency of the wheelsets depend on the longitudinal acceleration of the locomotive model (Figure 15). Remaining within the range of standard track parameters, the acceleration values varied from 0.5 to 1.0. For the straight track, the torsional vibration frequencies were practically the same for each of the wheelsets. This is illustrated by the blue line in Figure 15a. A resonant frequency of 500 Hz only appeared when the locomotive model was moving with an acceleration of 0.5.

In order to avoid resonant frequencies of vibrations, indicated by dotted lines in Figure 15, the locomotive model should increase its speed on straight track with an acceleration of more than 0.5, while in the case of a full curve of track with a radius of 300 m, this should be an acceleration in the value range of 0.7 to 0.83.

CONCLUSIONS

Based on the non-linear theory of wheel-rail rolling and the design of an actual high-speed electric locomotive, a three-dimensional model of such a vehicle equipped with an electro-mechanical individual drive system was built in the specialist Vi-Rail software. Non-linear wheel and rail profiles were taken into account, as well as the control of asynchronous traction motors using the PWM method. Simulation studies were performed both on straight track and on curved track with a small curve radius. In the article presented here, it was shown that a high-speed electric locomotive, driven by asynchronous motors in a hollow shaft arrangement and swing-out couplings, is capable of generating corrugation conditions on the surface of new and smooth rails on straight and curved track. It is noteworthy that the simulation model of the locomotive used for the study included a non-linear description of the wheel-rail contact and a mathematical model of the electrical part of the drive train. This made it possible to obtain very reliable data on the contact forces in the wheel-rail contact areas. Information on the values of the longitudinal tangential forces in the wheel-rail contact areas and the magnitudes of the electromagnetic moments generated by the traction motors were the input data needed to calculate the vertical and torsional vibration frequencies in the wheel-set-rail system. It was shown that during the transmission of driving moments to the axles of the wheelsets, cyclic, vertical and longitudinal loads on the given rail area are exerted by successive wheels. This confirmed that the excitations generated by the running locomotive drive train are similar in nature to those generated by corrugated rails. The authors of this paper plan to continue their research as it relates to the dynamic effects of corrugations already present on the rails on the drivetrain and other structural components of a high-speed electric locomotive.

REFERENCES

1. Bednarek, W. Zużycie faliste szyn toru kolejowego. *Archiwum Instytutu Inżynierii Lądowej* 2015; 20: 8-23.
2. Wang, Z., Lei, Z. Sensitivity Analysis for Influence Parameters of Rail Corrugation Characteristics in Metro Straight Section. *Advances in Science and Technology Research Journal* 2021; 15(4): 110–117. DOI: 10.12913/22998624/142034.
3. Chen, G. Friction-Induced Vibration of a Railway Wheelset-Track System and Its Effect on Rail Corrugation. *MDPI, Lubricants* 2020; 8: 18. DOI: 10.3390/lubricants8020018.
4. Xu, J., Wang, K., Liang, X. et al. Influence of viscoelastic mechanical properties of rail pads on wheel and corrugated rail rolling contact at high speeds. *Tribology International* 2020; 151. DOI: 10.1016/j.triboint.2020.106523.
5. Li, S. Mechanisms of short pitch rail corrugation. Dissertation for the purpose of obtaining the degree of doctor at Delft University of Technology, 2022. DOI: 10.4233/uuid:ee0e14ec-c4b2-4bcf-81cf-d09c3bb8b8c1.
6. Chen, Z., Zhang, J., Wang, K., Liu, P. Nonlinear dynamic responses of locomotive excited by rail corrugation and gear time-varying mesh stiffness. *Vilnius Gediminas Technical University, Transport* 2022; 37(6): 383–397. DOI: 10.3846/transport.2022.17065.
7. Marciniak, M., Nowak, S. Konstrukcja elektrycznej uniwersalnej jednosystemowej lokomotywy typu 113E-EU 11 dla Polskich Kolei Państwowych. *Pojazdy Szynowe* 1999; 1: 30-39.
8. Matej, J. Modelowanie i badanie dynamiki układu napędowego szybkobieżnego pojazdu szynowego. Praca statutowa nr 504/A/1153/2310/000, Instytut Pojazdów, Politechnika Warszawska, 2001, opracowanie wewnętrzne.
9. VI-Rail 18.0 Documentation. VI-grade engineering software & services, 2018.
10. Madej, J. Projektowanie mechanizmów napędowych pojazdów szynowych. WKŁ, Warszawa 1988.